Antimalarial 4(1H)-pyridones bind to the Q_i site of cytochrome bc_1

Michael J. Capper[a], Paul M. O'Neill[b], Nicholas Fisher[c,1], Richard W. Strange[a], Darren Moss[c], Stephen A. Ward[c], Neil G. Berry[b], Alexandre S. Lawrenson[b], S. Samar Hasnain[a,2], Giancarlo A. Biagini[c,2], and Svetlana V. Antonyuk[a,2]

[a]Molecular Biophysics Group, Institute of Integrative Biology, Faculty of Health and Life Sciences, University of Liverpool, Liverpool L69 7ZB, United Kingdom; [b]Department of Chemistry, Faculty of Science and Engineering, University of Liverpool, Liverpool L69 7ZB, United Kingdom; and [c]Research Centre for Drugs and Diagnostics, Liverpool School of Tropical Medicine, Liverpool L3 5QA, United Kingdom

Edited* by Gregory A. Petsko, Weill Cornell Medical College, New York, NY, and approved December 3, 2014 (received for review August 28, 2014)

Cytochrome bc_1 is a proven drug target in the prevention and treatment of malaria. The rise in drug-resistant strains of *Plasmodium falciparum*, the organism responsible for malaria, has generated a global effort in designing new classes of drugs. Much of the design/redesign work on overcoming this resistance has been focused on compounds that are presumed to bind the Q_o site (one of two potential binding sites within cytochrome bc_1) using the known crystal structure of this large membrane-bound macromolecular complex via in silico modeling. Cocrystallization of the cytochrome bc_1 complex with the 4(1H)-pyridone class of inhibitors, GSK932121 and GW844520, that have been shown to be potent antimalarial agents in vivo, revealed that these inhibitors do not bind at the Q_o site but bind at the Q_i site. The discovery that these compounds bind at the Q_i site may provide a molecular explanation for the cardiotoxicity and eventual failure of GSK932121 in phase-1 clinical trial and highlight the need for direct experimental observation of a compound bound to a target site before chemical optimization and development for clinical trials. The binding of the 4(1H)-pyridone class of inhibitors to Q_i also explains the ability of this class to overcome parasite Q_o-based atovaquone resistance and provides critical structural information for future design of new selective compounds with improved safety profiles.

malaria | cytochrome bc_1 | drug discovery | *Plasmodium falciparum* | membrane protein

Malaria is a major health problem in many parts of the world. In 2012 there were an estimated 219 million cases, from which there were over half a million deaths, the majority of which were pregnant women and children under 5 (1). Eradication programs have had some success in reducing malaria mortality through targeting the mosquito vector *Anopheles gambiae* and the development of a *Plasmodium* vaccine continues to show promise (2–4). Despite this success, incidence of chloroquine, artemisinin, and multidrug resistant strains of the *Plasmodium* parasite and of *Plasmodium falciparum*, the most lethal strains of malaria, have been reported and appear to be rising (5–7). Individual compounds used in monotherapy frequently suffer resistance, resulting in the need for expensive combinatorial treatments (8–10). This situation calls for new, cost-effective, drugs that can contribute toward more effective treatment and eventual eradication.

Cytochrome bc_1 (ubiquinol: cytochrome *c* oxidoreductase; complex III) is a major drug target for the treatment and prevention of malaria, and in the treatment of toxoplasmosis (8, 11). Cytochrome bc_1 is a dimeric multisubunit electron transport protein embedded in the inner-mitochondrial membrane (12–14). There are three catalytic subunits: cytochrome *b*, cytochrome c_1, and the Rieske iron–sulfur protein, which are present in all bc_1 complexes (12). The complex forms part of the respiratory chain and acts to transport H^+ into the intermembrane space through the oxidation and reduction of ubiquinone in the modified Q cycle (12, 15, 16). The Q cycle requires two distinct binding sites for the reduction and oxidation of ubiquinol and ubiquinone. Both sites are located within cytochrome *b*; the Q_o site acts to oxidize ubiquinol near the intermembrane space (17), and the Q_i site binds and reduces ubiquinone near the mitochondrial matrix. In *P. falciparum*, cytochrome bc_1 is essential to ensure a pool of oxidized ubiquinone for use by dihydroorotate dehydrogenase (DHODH) in pyrimidine biosynthesis; inhibition of cytochrome bc_1 or DHODH leads to parasite death (18, 19). Atovaquone, a hydroxynapthoquinone (Fig. 1), binds cytochrome bc_1 at the Q_o site (20, 21). It is used as a fixed-dose combination with proguanil (marketed as Malarone) for treating children and adults with uncomplicated malaria or as chemoprophylaxis for preventing malaria in travelers. In the United States, between 2009 and 2011, Malarone prescriptions accounted for 70% of all antimalarial pretravel prescriptions (22).

Several mutations, giving rise to atovaquone-resistant strains of *P. falciparum* and *Toxoplasma gondii*, have been reported since the turn of the century (23–27). These mutations arise in the Q_o pocket and prevent atovaquone from binding (28). A recent X-ray structure of cytochrome bc_1 from *Saccharomyces cerevisiae* has shown atovaquone bound in the catalytic Q_o site, offering explanation for the cross-species resistance (20). Many different classes of compound have been investigated as potential drugs and much work has focused on inhibition of the Q_o site (23, 29–32). The 4(1H)-pyridones have been researched for their antimalarial properties since the 1960s, based on the compound clopidol (33, 34) (Fig. 1). GW844520 produced by GlaxoSmithKline (GSK) was found to have excellent antimalarial drug properties, even against

Significance

X-ray crystallography greatly benefits drug discovery work by elucidating information about the binding of drug compounds to their target. Using this information, changes to the compounds can be made in a process known as rational drug design. Cytochrome bc_1 is a proven drug target in the treatment and prevention of malaria, a disease that kills over half a million people each year and many compounds have been developed to inhibit cytochrome bc_1. Here we show the binding of two such compounds in X-ray crystal structures, which reveal an unexpected binding site. This work opens up a new area for antimalarial research and reinforces the need for structural information in drug design.

Author contributions: P.M.O., S.S.H., G.A.B., and S.V.A. designed research; M.J.C., N.F., R.W.S., D.M., N.G.B., A.S.L., G.A.B., and S.V.A. performed research; P.M.O. and S.A.W. contributed new reagents/analytic tools; M.J.C. and S.V.A. analyzed data; and M.J.C., P.M.O., N.G.B., S.S.H., G.A.B., and S.V.A. wrote the paper.

The authors declare no conflict of interest.

*This Direct Submission article had a prearranged editor.

Freely available online through the PNAS open access option.

Data deposition: The atomic coordinates and structure factors have been deposited in the Protein Data Bank, www.pdb.org (PDB ID codes 4D6T and 4D6U).

[1]Present address: MSU–DOE Plant Research Laboratory, Michigan State University, East Lansing, MI 48824.

[2]To whom correspondence may be addressed. Email: s.s.hasnain@liverpool.ac.uk, antonyuk@liverpool.ac.uk, or biagini@liverpool.ac.uk.

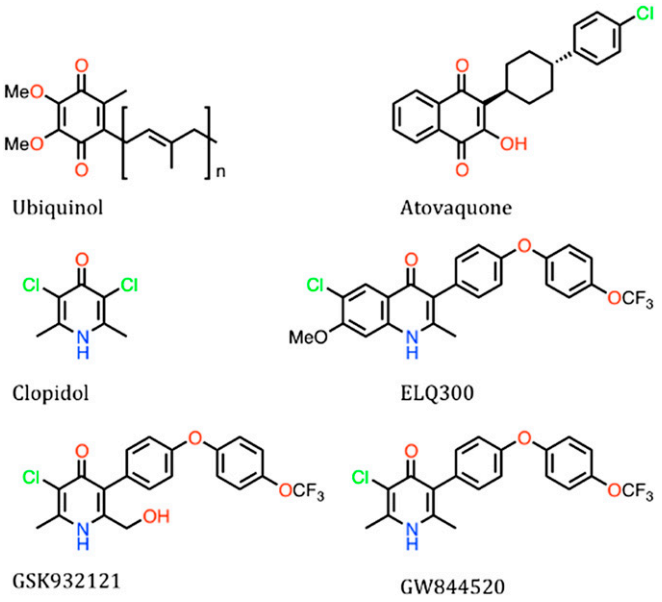

Fig. 1. Chemical structures of relevant compounds. Ubiquinol binds both the Q_o and Q_i site of cytochrome bc_1 in the modified Q cycle. Atovaquone, a hydroxynapthoquinone, is a known binder of the cytochrome bc_1 Q_o site. Clopidol is a known treatment for malaria and is the basis for the pyridone class of compound, including GW844520 and GSK932121. GSK932121 has a substituted alkyl group located on the head compared with GW844520.

atovaquone-resistant parasites, but had to be withdrawn from development due to unexpected toxicity (35). GSK932121 was also found to have strong antimalarial properties, including against atovaquone-resistant parasites (36), and progressed to a first time in human (FTIH) study. However, during the FTIH study, a phosphate-prodrug backup of GSK932121 was observed to result in unexpected acute toxicity in rats after oral administration, which was subsequently replicated by dosing GSK932121 alone through i.p. administration at similar exposure levels to those achieved with its prodrug. The observed acute toxicity resulted in the immediate termination of the FTIH study and was attributed to cardiotoxicity, possibly via the inhibition of the mammalian bc_1 (37). It was concluded that these compounds may bind to the Q_o site of cytochrome bc_1 in a novel way to overcome atovaquone resistance.

The Q_i site of cytochrome bc_1 has been far less explored in the search for antimalarial compounds and only the binding of a few compounds has been visualized directly (38–40). Several compounds have been suggested to bind the Q_i site, including potential antimalarial compounds, but due to lack of structural information have not been pursued vigorously (41). Here we provide the structure of bovine heart cytochrome bc_1 complex with 4(1H)-pyridone compounds, GW844520 and GSK932121. The crystallographic structures provide clear evidence of these compounds unexpectedly bound in the Q_i site. This discovery explains the ability of this class to overcome parasite atovaquone resistance and provides critical structural information for the future design of new selective compounds with reduced/no toxicity.

Results

The Pyridones GSK932121 and GW844520 Bind to Q_i Site of Cytochrome bc_1. Structures of cytochrome bc_1 complexes from multiple organisms bound to various compounds have been previously published (14, 38, 42, 43). The majority of these compounds are bound to the Q_o site in various conformations (44). The pyridones GSK932121 and GW844520 had been suggested to bind bovine cytochrome bc_1 at the Q_o site through mutation and chemical-binding studies (29). Electron density was clearly visible within the Q_i site and each of the pyridones fit accurately (Fig. 2). The Q_i binding site is located within the transmembrane region of cytochrome bc_1 and is formed by residues of transmembrane helices A, D, and E as well as helix a and the heme b_H (14, 45). It is accessible through a hydrophobic channel, which terminates at heme b_H and several polar residues (Fig. 3). The binding of both GSK932121 and GW844520 appears very similar with the head group of both molecules binding close to heme b_H and the tail extending out of the channel away from the heme (Fig. 3*C*).

The head of the compound was placed unambiguously in a plane according to the omit Fo-Fc density and oriented so that the amine of the pyridone and the N of His201 on helix D (Fig. 2) were within bonding range. The carbonyl of both GW844520 and GSK932121 was within 3.5 Å of both Ser35 on loop A and OD1 of Asp228 on loop E to allow forming of H bonds (Fig. 3*C*). After refinement with the compounds, additional electron density became visible, allowing positioning of the triflouromethyl tail group between Met190 and Met194. There was visible density along the first phenyl group of the hydrophobic tail of each compound. Residues Phe18, Leu21, and Leu197 form a tight hydrophobic pocket around the aromatic rings of the pyridone tail while Phe220 appears to form a stacking interaction with the head group suggesting hydrophobic interactions provide a large part of the binding energy (Fig. 3*C*). No density was visible in the Q_o site confirming that these compounds bind solely to the Q_i site.

Residue Differences in Binding Pocket. The protein sequence alignment of bovine, human, and *P. falciparum* cytochrome *b* shows a fairly conserved Q_i binding site (Fig. 4*C*). However, there are differences in the N-terminal region of cytochrome *b* between the mammalian protein and the *Plasmodium* homolog. The protein is shorter in both *T. gondii* and *Plasmodia*. Both Phe18 and Leu21 of the surface loop before helix A, which forms a hydrophobic pocket around the aromatic tail of the 4(1H)-pyridones, are replaced with Leu and Tyr, respectively, in both *P.*

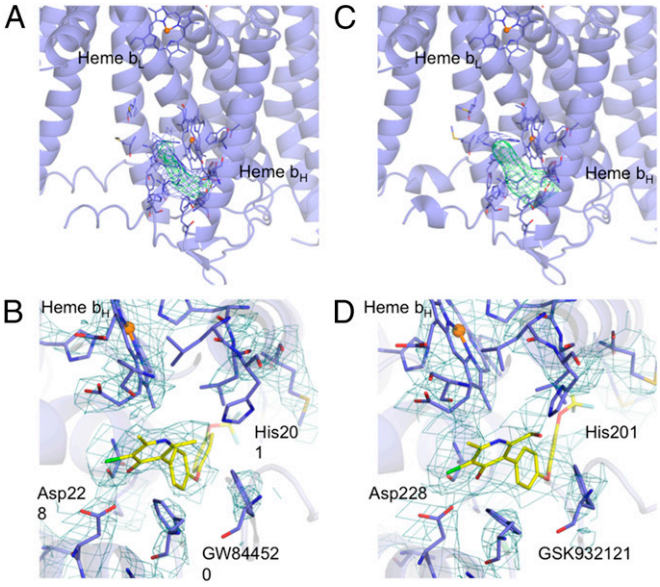

Fig. 2. Cytochrome bc_1 Q_i binding site occupied by 4(1H)-pyridones. The Fo-Fc and 2Fo-Fc electron density maps are shown in green and blue at 3σ and 1σ, respectively. (*A* and *B*) Present data for the GW844520 complex; (*C* and *D*) for the GSK932121 complex. The electron density is clearly visible around compound and surrounding residues involved in binding, including heme b_H, His203, and Phe222.

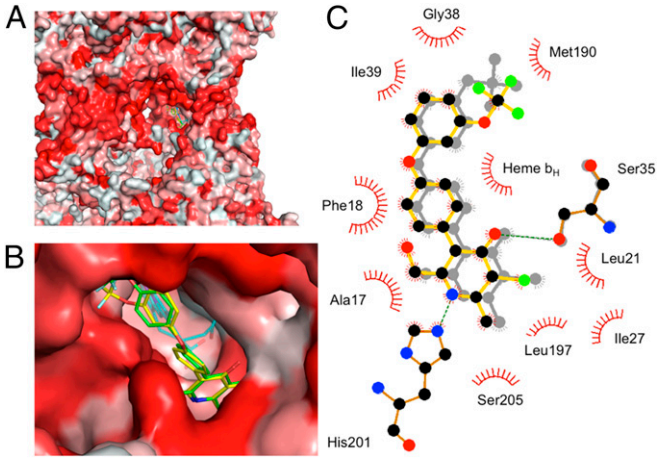

Fig. 3. Binding of GW844520 and GSK932121 within the hydrophobic Q_i cavity. (*A*) Surface view of cytochrome bc_1 in complex with GSK932121 (green) and GW844520 (yellow) colored by hydrophobicity: more hydrophobic residues are red, more polar residues are white. (*B*) View of the binding site: the hydrophobic tail of each compound lies along the cavity, keeping close to the hydrophobic surface, whereas the head binds near the heme in a polar environment. (*C*) Two-dimensional pharmacophore of the various interactions between the Q_i binding site and both pyridone compounds: GW844520 in the foreground, GW844520 in gray in the rear. Specific atoms are colored accordingly: carbon in black, oxygen in red, nitrogen in blue, and halogens in green (produced using Ligplot) (53).

falciparum and *T. gondii*, which would suggest large differences in the binding around the tail groups of both compounds. Ala191 allows a large opening in the cavity toward the terminus of the Q_i site but is replaced by a Cys residue in the parasite. Both Met190 and Met194 are nonconserved between all of the sequences aligned, whereas Gly204 and Ser205 are conserved. Ser205 has been shown to be involved in the binding of ubiquinone (44). Phe220 is conserved across cytochrome *b* sequences and is thought to be important in forming an interaction with the aromatic pyridone head group, whereas Leu201 located on the opposite side to Phe220 is conserved in both the parasite and human protein.

Cellular Toxicity of GW844520 and GSK932121 Is Associated with Mitochondrial Dysfunction. Mitochondrial toxicity can be identified by the differing responses observed for HepG2 cells grown in glucose-containing media, which favors glycolysis, or galactose-containing media, which promotes reliance upon oxidative phosphorylation (46). As an exemplar, the toxicity of tamoxifen is observed to be unaltered by a change of growth media, as is expected for a compound with no known mitochondrial toxicity (Fig. 5*A*). Conversely, the mitochondrial complex I (NADH: quinone oxidoreducatse) inhibitor rotenone is not significantly toxic in glucose media but demonstrates severe toxicity in galactose media (Fig. 5*B*), thus indicting disruption of oxidative phosphorylation. Both GW844520 and GSK932121 (Fig. 5 *C* and *D*) displayed significantly enhanced toxicity in the galactose medium, indicative of mitochondrial-based toxicity. However, the next generation 4(1H)-quinolone-3-diarylether ELQ 300 (30) and 2-aryl quinolone SL-2-25 (47) did not show significant enhancement of toxicity in galactose-grown HepG2 (Fig. 5 *E* and *F*).

Molecular Docking. Molecular docking was performed using the coordinates of the cocrystallized structures of bovine bc_1 complex reported here. A protocol was developed and validated, which is able to reproduce the crystallographic binding modes of both GW844520 and GSK932121 (Fig. 6). The docked model and experimental structures showed excellent agreement (rmsd < 2 Å) for both GSK932121 and GW844520 (Fig. 6). This protocol was also applied to predict the binding poses for antimycin A, a compound known to bind to the Q_i site, as a control (42). Atovaquone that has been shown not to bind to the Q_i site was also used as a control. The docking for antimycin A was able to reproduce the X-ray crystallographic binding pose (rmsd 1.67 Å) and forms a very similar array of noncovalent interactions with the protein as GSK932121 and GW844520. In contrast, atovaquone did not produce consistent docking poses in the Q_i binding site (data not shown). These facts indicate the robust nature of the docking protocol used in the light of new structures and show the potential for its use for further development of compounds. The next generation compounds, namely ELQ 300 and SL-2-25, showed their binding to the Q_i site.

Discussion

The structural details of cocrystallized bovine cytochrome bc_1 complex and compounds GW844520 and GSK932121 show similar binding modes in the Q_i pocket (Fig. 2), suggesting that this binding mode is likely to prevail in the family of 4(1H)-pyridone compounds. The formation of hydrogen bonds between several residues and the head group of each compound means that these are strongly bound at the end of the channel, 12 Å away from the center of heme b_H. The head forms several electrostatic interactions. Nε2 of His201 is pointed directly at the amide of the pyridone head and is separated by 3.3 Å. Ser205 and Asp228 on helix E are 2.9 Å and 2.7 Å from the carbonyl group, respectively, which is common among many Q_i binding ligands. These residues are also found to interact directly with the head of antimycin and ubiquinone, which lie in a similar position deep within this cavity (38, 42). The chlorine atom is 4.3 Å away from the carboxyl of Trp31 and is largely surrounded by aliphatic residues in a hydrophobic space. The change from a methyl group at position 6 in GW844520 to an alkyl group in GSK932121 shows little difference in the electron density; however, it does appear within 3 Å of the carbonyl of the peptide bond in Ala17. Ala17 forms part of the N-terminal region that

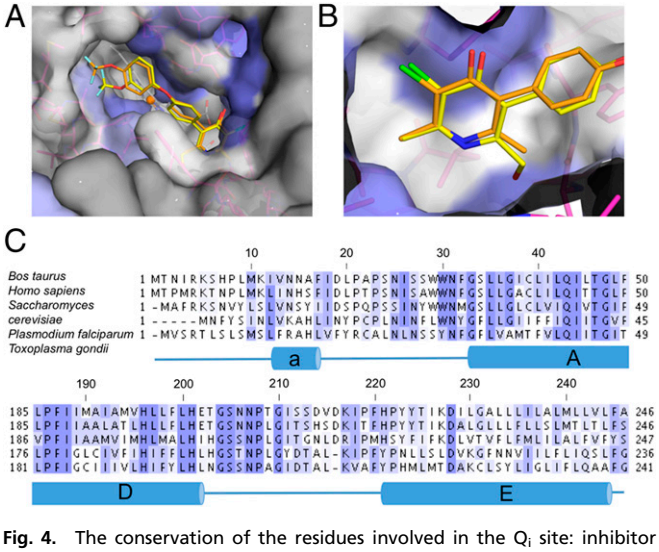

Fig. 4. The conservation of the residues involved in the Q_i site: inhibitor binding shows opportunities for future drug design. Residues fully conserved between human and malaria are colored in deep blue, partially conserved in light blue, and unconserved in white. Residues not involved in Q_i site binding are colored in gray. The structural details of (*A*) the tail binding region and (*B*) head binding for both GW844520 (orange) and GSK932121 (yellow). (*C*) Protein sequence alignment between bovine, human, *S. cerevisiae*, *P. falciparum*, and *T. gondii* showing conservation in the Q_i binding site. Scale at the *Top* is numbered according to bovine sequence.

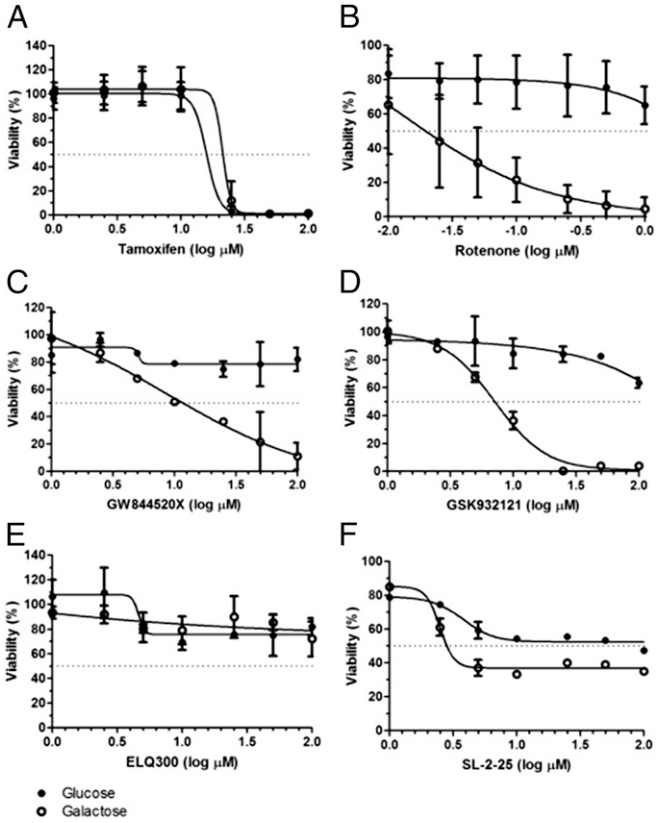

Fig. 5. Determining the site of toxicity of the 4(1H)-pyridones and next generation quinolones. By reversing the Crabtree effect using HepG2 cells grown on galactose, it is possible to demonstrate that compounds (*A*) tamoxifen, (*E*) ELQ 300, and (*F*) SL-2-25 do not greatly affect viability through oxidative phosphorylation. Compounds (*B*) rotenone, (*C*) GW844520, and (*D*) GSK932121 significantly disrupt oxidative phosphorylation. Data show averages from independent experiments ($n \geq 3$), ±SD. The IC_{50} values were determined using a four-parameter logistic function.

is not conserved in *Plasmodia* parasites (Fig. 4), which may help to explain differences in binding between mammalian and parasite complexes.

The tail of each compound proceeds away from heme b_H and directly down toward the entrance of the cavity between cytochrome bc_1 monomers. The tail region appears more flexible in GSK932121, perhaps due to alternate location of the trifluoromethyl group (Fig. 1) no longer being able to interact with Met194. Phe18 can be seen forming a stacking interaction with both phenyl rings of the tail, which may help fix the pyridone compounds in place as opposed to the lack of density that was seen in ubiquinone-bound structures (38). This would help explain the increased strength of binding in the pyridones compared with ubiquinone.

Reversing the Crabtree effect in HepG2 cells by switching to a galactose carbon source can be shown to clearly discriminate between nonmitochondrial (e.g., tamoxifen; Fig. 5*A*) and mitochondrial (e.g., rotenone; Fig. 5*B*) inhibitors. Consistent with the presented cocrystallized structural data of GSK932121 and GW844520 bound to bovine bc_1 and the hypothesis that the acute in vivo toxicity seen in this pyridone class is of mitochondrial origin (37), both GSK932121 and GW844520 display significantly enhanced toxicity in galactose media (Fig. 5 *C* and *D*). The next generation 4(1H)-quinolone-3-diarylether ELQ 300 (30) and 2-aryl quinolone SL-2-25 (47) did not show significant enhancement of toxicity in galactose-grown HepG2 (Fig. 5 *E* and *F*), suggesting that these preferentially target *Plasmodium* bc_1. These data are consistent with human and bovine bc_1 sensitivity data previously reported (30, 47).

As noted, it has been generally accepted that the 4(1H)-pyridone class, e.g., GW844520, targets the Q_o oxidation site of the bc_1 complex, via analogy with the mechanism of action of the Q_o targeted antimalarial atovaquone, and indeed models of the pyridone/bc_1 Q_o interaction of these molecules have been previously described (33). The next generation bc_1 inhibitor quinolone, ELQ 300, was designed by replacement of the pyridone unit of GW844520, with a quinolone group as shown (Fig. 1), and the close similarity of these two antimalarials would suggest, based on the GSK model, that the Q_o site is the likely molecular target. Here, using docking, we show that ELQ 300 and SL-2-25 bind well at the Q_i site, suggesting an alternative target site/mechanism to atovaquone.

This modeling observation is consistent with our recent studies on the quinolone 1-hydroxy-2-dodecyl- 4(1H)quinolone (HDQ) in yeast models (41). Introduction of point mutations into the Q_i site, namely G33A, H204Y, M221Q, and K228M, markedly decreased HDQ inhibition; by contrast, known inhibitor resistance mutations at the Q_o site did not cause HDQ resistance. A recent study in *T. gondii* showed that mutations at the Q_i site of yeast cytochrome *b* reduced the growth inhibition effect of ELQ 271 (48). Taken together, these data indicate that the Q_i site of the bc_1 complex is the likely target for a number of next generation ubiquinone-mimicking antimalarials that are not cross-resistant with atovaquone. In support of this finding, the docking poses of both ELQ 300 and SL-2-25 molecules were similar, with the quinolone head groups both bound at the end of the pocket defined by His201, Ser205, Asp228, and Ser35 of cytochrome *b* with the long hydrophobic tails of the compounds directed toward the region defined by Met190, Met194, and Ile42 (analogous with GSK932121 and GW844520).

Although cytochrome *b* appears to be highly conserved across phyla, the differences between cytochrome *b* in members of the *Plasmodia* family compared with human appear significant from sequence alignment. The N-terminal region appears considerably shorter, which is likely to result in a considerably different opening to the Q_i cavity and binding site. This difference in primary structure could open up the tail region of the pyridone compounds to more specific binding, preventing cross-reactivity between pathogen and host. Interestingly, the fluorine atom of GW844520 appears bound next to Met194, which is only present in the bovine cytochrome *b* protein. This could explain the higher IC_{50} reported for bovine cytochrome bc_1 compared with the human (29), despite the high conservation in their sequence. In the *Plasmodia* protein, Met194 is substituted by a Phe residue (Fig. 4*C*), which could allow for specific compound modifications to be made to increase binding. Phe18 is another promising tail region residue for drug design, as in the *Plasmodia* sequence, it is substituted for a Leu. Within the head group of the binding site, Ser205, which binds the carbonyl of both pyridone molecules, is replaced with a Phe residue. It is difficult to estimate what would

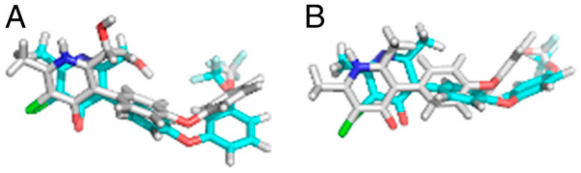

Fig. 6. Comparison of the ligand's docking poses with the conformation from X-ray crystal structures (*A*) GSK932121 and (*B*) GW844520. (rmsd GSK932121 1.634 Å and GW844520 1.762 Å). Molecules are rendered as sticks colored by atom type (carbon docking, light gray; carbon crystal structure, cyan; chlorine, green; oxygen, red; and fluorine, light blue).

happen within the binding site, but this difference may go some way to explaining why binding within the parasite is an order of magnitude stronger than in bovine (29).

Work on improving the clinically promising 4(1H)-pyridones so far has lacked structural information (33, 34). The elucidation of 4(1H)-pyridone binding within the Q_i site of mitochondrial cytochrome bc_1 complex provides for the first time to our knowledge an opportunity for rational drug design to increase selectivity against *Plasmodia* parasites toward novel treatments and reducing transmission. The overwhelming importance of direct observation of drug leads at their target sites is highlighted in this study. In situ visualization of drug candidates by experimental structural methods such as X-ray crystallography should be built in as the gold standard for validation of binding of these compounds before optimization in a drug-discovery pipeline.

Materials and Methods

Preparation of Crude Protein. Isolation of crude mitochondria was carried out as previously reported in the following method (14). Briefly, bovine heart muscle was homogenized in a Waring blender and added at a ratio of 2 L buffer (250 mM sucrose; 20 mM K_2HPO_4; 2 mM succinic acid; 0.5 mM EDTA) per 500 g of muscle tissue. The homogenate was subjected to centrifugation at 1,500 × *g* for 20 min and the supernatant was then further centrifuged at 23,500 × *g* for 20 min. The pellet, containing bovine mitochondria, was collected and washed in wash buffer 1 (50 mM KPi pH 7.5; 0.1 mM PMSF). The mitochondrial pellet was resuspended in wash buffer 2 (50 mM KPi pH 7.5; 250 mM NaCl; 3 mM NaN_3; 0.1 mM PMSF). The amount of protein was quantified using a BCA (bicinchoninic acid) assay (Pierce). The remaining solution was centrifuged at 180,000 × *g* for 60 min and the pellet was resuspended in the same wash buffer, with the addition 0.1 mg n-dodecyl β-D-maltopyranoside (DDM) per 1 mg of protein. The solution was centrifuged again under the same conditions. The pellet was then resuspended with the addition of 0.9 mg DDM per 1 mg of protein and centrifuged under the same conditions once more. The supernatant containing solubilized membrane proteins was collected.

Purification of Cytochrome bc_1. The solubilized proteins were loaded on a DEAE-Sepharose CL-6B (Sigma-Aldrich) column (approximately 50 mL) preequilibrated with buffer A (50 mM KPi pH 7.5; 250 mM NaCl; 0.03% DDM; 3 mM NaN_3), then washed with 2 column volumes (CVs) of buffer A and eluted along a linear gradient from 250 mM to 500 mM NaCl. The cytochrome bc_1-containing fractions were pooled together before being diluted twofold with buffer C (50 mM KPi pH 7.5; 0.03% DDM; 3 mM NaN_3). The protein solution was then applied to a hydroxyapatite (Bio-Rad) column (approximately 15 mL), washed with 10 CVs of buffer C before elution with the gradient from 50 mM to 1 M KPi (pH 7.5). Fractions containing cytochrome bc_1 were then concentrated to approximately 500 μL, using an Amicon Ultra-15 (Millipore, MWCO 100,000). The concentrated protein was then applied to a Sephacryl-S300 (GE Healthcare) column (approximately 120 mL) preequilibrated with buffer D (25 mM KPi (pH 7.5); 100 mM NaCl; 0.015% DDM; 3 mM NaN_3) and eluted at a flow rate of 0.5 mL/min.

Crystallization of Cytochrome bc_1. Inhibitors dissolved in DMSO solution at a stock concentration of 10 mM were added to cytochrome bc_1 in 10-fold molar excess and incubated at 4 °C for one hour. Remaining DMSO and inhibitors were removed via buffer exchange on an Amicon Ultra-4 (Millipore, MWCO 100,000) and the protein was concentrated to 30 mg/mL in 25 mM KPi (pH 7.5), 100 mM NaCl, 0.015% DDM, 3 mM NaN_3. Crystallization was preformed at 4 °C by sitting drop vapor diffusion method over reservoir solution containing 50 mM KPi (pH 6.4–7.2), 100 mM NaCl, 3 mM NaN_3, 10–13% PEG4000 and 0.14% 6-O-(*N*-Heptylcarbamoyl)-methyl-α-D-glucopyranoside (HECAMEG). Drops were made to 10 μL with 1:1 ratio of protein to precipitant. Crystals appeared overnight among precipitation and were allowed to grow before being flash frozen in 25% (vol/vol) glycerol.

Data Collection, Processing, Model Building, and Refinement. Data collection statistics can be found in Table 1. Multiple crystals from the same drop were tested at 100 K using a home source FRE+ and Mar225 CCD at the Barkla X-ray Laboratory in Liverpool before transport to SOLEIL PROXIMA1 and Diamond Light Source IO4 beamline. Datasets from multiple crystals belonging to the same $P6_5$ space group and unit cell were collected at 100 K using a 1-Å beam before being scaled and merged together using DENZO in the HKL2000 suite (49). Molecular replacement was carried out using pdb: 1PPJ as a starting model (42) in MOLREP (50) followed by rigid body refinement in Refmac5 (51). Cycles of automatic refinement were carried out using Refmac 5 with Prosmart restraints and manual input was done with COOT (52). Ligands were produced in JLigand and added manually (53). Pyridones were placed in both Q_i sites of the dimer with equal confidence. Two-dimensional pharmacophores of both GSK932121 and GW844520 were produced using LigPlot+ (54).

Sequence Alignment. Protein sequences for cytochrome *b* of various species were taken from the UniProtKB and aligned using ClustalOmega (55). The alignment was visualized using JalView 2.8 and additional annotations were added using GIMP.

Reverse Crabtree-Effect Cellular Toxicity Studies. Cellular toxicities were determined based on the method of Marroquin et al. (46) modified by Warman et al. (56), Briefly, HepG2 cells cultured in glucose media (high-glucose DMEM containing 25 mM glucose, 1 mM sodium pyruvate, 5 mM Hepes, 10% FBS, and 100 μg/mL penicillin/streptomycin) or galactose media (as per glucose media but using glucose-free DMEM) were added to 96-well plates (100 μL, 1×10^4 cells per well) and incubated for 24 h at 37 °C. The test compounds were added and incubation continued for an additional 24 h. The plates were subsequently incubated for 2 h in the presence of 1 mg/mL 3-(4,5-dimethylthiazol-2-yl)-2,5-diphenyltetrazolium bromide solution. Solubilization buffer, consisting of 50% (vol/vol) *N*,*N*-dimethylformamide and 20% (wt/vol) SDS, was added before well absorbance at 560 nm was measured using a Varioskan plate reader (Thermo Scientific). Experiments were performed in triplicate and repeated on three or more independent occasions. The IC_{50} values were determined using a four-parameter logistic function.

Chemistry. ELQ 300 was prepared as described by Nilsen et al. using (4-(trifluoromethoxy) phenyl) boronic acid as starting material (57). GW844520 was prepared as outlined by Yeates et al. (34). GSK932121 was prepared in six steps from intermediate 2, according to Bueno et al. (33). (For the synthesis of 2, see the route developed by Liu et al. (58).

Molecular Docking. Three-dimensional structures of the compounds docked were created via energy minimization using the Merck molecular force field

Table 1. Data collection and refinement statistics

Data collection and refinement	bc_1-GW844520	bc_1-GSK932121
Space group	P 6_5	P 6_5
Cell dimensions		
a, *b*, *c*, Å	129.9. 129.9, 722.2	129.5, 129.5, 719.9
α, β, γ, °	90, 90, 120	90, 90, 120
Resolution (Å)	50–3.55 (3.68–3.58)	50–4.09 (4.25–4.09)
R_{merge}	23.8 (100)	14.7 (50.6)
$I/\sigma I$	7.01 (1.83)	6.03 (1.78)
Completeness (%)	100 (100)	80.7 (51.5)*
Redundancy	8 (7)	3.2 (2.6)
Refinement		
Resolution, Å	50–3.55	50–4.09
No. reflections	77,417	40,901
R_{work}/R_{free}	20.60/25.16	22.33/27.11
Nonhydrogen atoms		
Protein	30,376	30,365
4(1H)-Pyridone	28	29
Other ligands	686	688
B factors		
Protein	141.90	170.01
4(1H)-Pyridone	157.90	173.20
Other ligands	135.54	159.57
Rms deviations		
Bond lengths, Å	0.011	0.013
Bond angles, °	1.695	1.454
PDB access codes	4D6T	4D6U

*Values in parentheses are for highest-resolution shell. The density supporting the positioning of the compound is still strong despite the low completeness.

(MMFF) 94 (59) within the SPARTAN '08 1.2.0 package. (Spartan '08, Wavefunction, 2008; www.wavefun.com, accessed June 30, 14). All molecular docking was performed using the GOLD docking suite version 5.2 (60–62). A genetic algorithm (GA) using piecewise linear potential (PLP) as the fitness function was used for all docking calculations. Ten independent GA runs were performed for each ligand. Default settings were used except the "allow early termination" setting in the "fitness and search option" was turned off.

ACKNOWLEDGMENTS. We thank the staff and management of SOLEIL and Diamond for provision of the crystallographic facilities at their synchrotron centres. Use of SOLEIL was part funded by the European Community's Seventh Framework Program (FP7/2007-2013) under BioStruct-X Grant 283570 and Proposal 2370/5437 (to S.V.A. and S.S.H.). G.A.B., P.M.O., and S.A.W. acknowledge support from the Medical Research Council (Grant 100278) and the Wellcome Trust (WT078285). S.V.A. acknowledges the support from Wellcome Trust (097826/Z/11/Z).

1. WHO (2012) *WHO|World Malaria Report 2012* (World Health Organization, Geneva).
2. Murray CJL, et al. (2012) Global malaria mortality between 1980 and 2010: A systematic analysis. *Lancet* 379(9814):413–431.
3. Mendis K, et al. (2009) From malaria control to eradication: The WHO perspective. *Trop Med Int Health* 14(7):802–809.
4. Greenwood BM, et al. (2008) Malaria: Progress, perils, and prospects for eradication. *J Clin Invest* 118(4):1266–1276.
5. Kessl JJ, Meshnick SR, Trumpower BL (2007) Modeling the molecular basis of atovaquone resistance in parasites and pathogenic fungi. *Trends Parasitol* 23(10):494–501.
6. Breman JG (2001) The ears of the hippopotamus: Manifestations, determinants, and estimates of the malaria burden. *Am J Trop Med Hyg* 64(1-2, Suppl):1–11.
7. Färnert A, et al. (2003) Evidence of Plasmodium falciparum malaria resistant to atovaquone and proguanil hydrochloride: Case reports. *BMJ* 326(7390):628–629.
8. Looareesuwan S, Chulay JD, Canfield CJ, Hutchinson DBA; Malarone Clinical Trials Study Group (1999) Malarone (atovaquone and proguanil hydrochloride): A review of its clinical development for treatment of malaria. *Am J Trop Med Hyg* 60(4):533–541.
9. Kremsner PG, Krishna S (2004) Antimalarial combinations. *Lancet* 364(9430):285–294.
10. Mutabingwa TK, et al. (2005) Amodiaquine alone, amodiaquine+sulfadoxine-pyrimethamine, amodiaquine+artesunate, and artemether-lumefantrine for outpatient treatment of malaria in Tanzanian children: A four-arm randomised effectiveness trial. *Lancet* 365(9469):1474–1480.
11. Fleck SL, Pudney M, Sinden RE (1996) The effect of atovaquone (566C80) on the maturation and viability of Plasmodium falciparum gametocytes in vitro. *Trans R Soc Trop Med Hyg* 90(3):309–312.
12. Berry EA, Guergova-Kuras M, Huang L-S, Crofts AR (2000) Structure and function of cytochrome bc complexes. *Annu Rev Biochem* 69:1005–1075.
13. Rieske JS, Hansen RE, Zaugg WS (1964) Studies on the Electron Transfer System. *J Biol Chem* 239:3017–3022.
14. Iwata S, et al. (1998) Complete structure of the 11-subunit bovine mitochondrial cytochrome bc1 complex. *Science* 281(5373):64–71.
15. Mitchell P (1976) Possible molecular mechanisms of the protonmotive function of cytochrome systems. *J Theor Biol* 62(2):327–367.
16. Crofts AR, et al. (1999) Mechanism of ubiquinol oxidation by the bc(1) complex: Role of the iron sulfur protein and its mobility. *Biochemistry* 38(48):15791–15806.
17. Berry EA, Huang L-S (2011) Conformationally linked interaction in the cytochrome bc (1) complex between inhibitors of the Q(o) site and the Rieske iron-sulfur protein. *Biochim Biophys Acta* 1807(10):1349–1363.
18. Srivastava IK, Vaidya AB (1999) A mechanism for the synergistic antimalarial action of atovaquone and proguanil. *Antimicrob Agents Chemother* 43(6):1334–1339.
19. Painter HJ, Morrisey JM, Mather MW, Vaidya AB (2007) Specific role of mitochondrial electron transport in blood-stage Plasmodium falciparum. *Nature* 446(7131):88–91.
20. Birth D, Kao W-C, Hunte C (2014) Structural analysis of atovaquone-inhibited cytochrome bc1 complex reveals the molecular basis of antimalarial drug action. *Nat Commun* 5:4029.
21. Fry M, Pudney M (1992) Site of action of the antimalarial hydroxynaphthoquinone, 2-[trans-4-(4′-chlorophenyl) cyclohexyl]-3-hydroxy-1,4-naphthoquinone (566C80). *Biochem Pharmacol* 43(7):1545–1553.
22. Nixon GL, et al. (2013) Antimalarial pharmacology and therapeutics of atovaquone. *J Antimicrob Chemother* 68(5):977–985.
23. Barton V, Fisher N, Biagini GA, Ward SA, O'Neill PM (2010) Inhibiting Plasmodium cytochrome bc1: A complex issue. *Curr Opin Chem Biol* 14(4):440–446.
24. Korsinczky M, et al. (2000) Mutations in Plasmodium falciparum cytochrome b that are associated with atovaquone resistance are located at a putative drug-binding site. *Antimicrob Agents Chemother* 44(8):2100–2108.
25. Fisher N, et al. (2012) Cytochrome b mutation Y268S conferring atovaquone resistance phenotype in malaria parasite results in reduced parasite bc1 catalytic turnover and protein expression. *J Biol Chem* 287(13):9731–9741.
26. Kessl JJ, Ha KH, Merritt AK, Meshnick SR, Trumpower BL (2006) Molecular basis of Toxoplasma gondii atovaquone resistance modeled in Saccharomyces cerevisiae. *Mol Biochem Parasitol* 146(2):255–258.
27. Srivastava IK, Morrisey JM, Darrouzet E, Daldal F, Vaidya AB (1999) Resistance mutations reveal the atovaquone-binding domain of cytochrome b in malaria parasites. *Mol Microbiol* 33(4):704–711.
28. Fisher N, Meunier B (2008) Molecular basis of resistance to cytochrome bc1 inhibitors. *FEMS Yeast Res* 8(2):183–192.
29. Biagini GA, et al. (2008) Acridinediones: Selective and potent inhibitors of the malaria parasite mitochondrial bc1 complex. *Mol Pharmacol* 73(5):1347–1355.
30. Nilsen A, et al. (2013) Quinolone-3-diarylethers: A new class of antimalarial drug. *Sci Transl Med* 5:177ra37.
31. Pidathala C, et al. (2012) Identification, design and biological evaluation of bisaryl quinolones targeting Plasmodium falciparum type II NADH:quinone oxidoreductase (PfNDH2). *J Med Chem* 55(5):1831–1843.
32. Edwards G, Biagini GA (2006) Resisting resistance: Dealing with the irrepressible problem of malaria. *Br J Clin Pharmacol* 61(6):690–693.
33. Bueno JM, et al. (2011) Potent antimalarial 4-pyridones with improved physicochemical properties. *Bioorg Med Chem Lett* 21(18):5214–5218.
34. Yeates CL, et al. (2008) Synthesis and structure-activity relationships of 4-pyridones as potential antimalarials. *J Med Chem* 51(9):2845–2852.
35. Xiang H, et al. (2006) Preclinical drug metabolism and pharmacokinetic evaluation of GW844520, a novel anti-malarial mitochondrial electron transport inhibitor. *J Pharm Sci* 95(12):2657–2672.
36. Jiménez-Díaz MB, et al. (2009) Improved murine model of malaria using Plasmodium falciparum competent strains and non-myelodepleted NOD-scid IL2Rgammanull mice engrafted with human erythrocytes. *Antimicrob Agents Chemother* 53(10):4533–4536.
37. Bueno JM, et al. (2012) Exploration of 4(1H)-pyridones as a novel family of potent antimalarial inhibitors of the plasmodial cytochrome bc1. *Future Med Chem* 4(18): 2311–2323.
38. Gao X, et al. (2003) Structural basis for the quinone reduction in the bc1 complex: A comparative analysis of crystal structures of mitochondrial cytochrome bc1 with bound substrate and inhibitors at the Qi site. *Biochemistry* 42(30):9067–9080.
39. Li H, Zhu X-L, Yang W-C, Yang G-F (2014) Comparative kinetics of Qi site inhibitors of cytochrome bc1 complex: Picomolar antimycin and micromolar cyazofamid. *Chem Biol Drug Des* 83(1):71–80.
40. Berry EA, et al. (2010) Ascochlorin is a novel, specific inhibitor of the mitochondrial cytochrome bc1 complex. *Biochim Biophys Acta* 1797(3):360–370.
41. Vallières C, et al. (2012) HDQ, a potent inhibitor of Plasmodium falciparum proliferation, binds to the quinone reduction site of the cytochrome bc1 complex. *Antimicrob Agents Chemother* 56(7):3739–3747.
42. Huang LS, Cobessi D, Tung EY, Berry EA (2005) Binding of the respiratory chain inhibitor antimycin to the mitochondrial bc1 complex: A new crystal structure reveals an altered intramolecular hydrogen-bonding pattern. *J Mol Biol* 351(3):573–597.
43. Hunte C, Koepke J, Lange C, Rossmanith T, Michel H (2000) Structure at 2.3 A resolution of the cytochrome bc(1) complex from the yeast Saccharomyces cerevisiae co-crystallized with an antibody Fv fragment. *Structure* 8(6):669–684.
44. Esser L, et al. (2004) Crystallographic studies of quinol oxidation site inhibitors: A modified classification of inhibitors for the cytochrome bc(1) complex. *J Mol Biol* 341(1):281–302.
45. Xia D, et al. (1997) Crystal structure of the cytochrome bc1 complex from bovine heart mitochondria. *Science* 277:60–66.
46. Marroquin LD, Hynes J, Dykens JA, Jamieson JD, Will Y (2007) Circumventing the Crabtree effect: Replacing media glucose with galactose increases susceptibility of HepG2 cells to mitochondrial toxicants. *Toxicol Sci* 97(2):539–547.
47. Biagini GA, et al. (2012) Generation of quinolone antimalarials targeting the Plasmodium falciparum mitochondrial respiratory chain for the treatment and prophylaxis of malaria. *Proc Natl Acad Sci USA* 109(21):8298–8303.
48. Doggett JS, et al. (2012) Endochin-like quinolones are highly efficacious against acute and latent experimental toxoplasmosis. *Proc Natl Acad Sci USA* 109(39):15936–15941.
49. Otwinowski Z, Minor W (1997) Processing of X-ray diffraction data collected in oscillation mode. *Macromol Crystallogr PT A* 276:307–326.
50. Vagin A, Teplyakov A (2010) Molecular replacement with MOLREP. *Acta Crystallogr D Biol Crystallogr* 66(Pt 1):22–25.
51. Murshudov GN, Vagin AA, Dodson EJ (1997) Refinement of macromolecular structures by the maximum-likelihood method. *Acta Crystallogr D Biol Crystallogr* 53(Pt 3): 240–255.
52. Emsley P, Cowtan K (2004) Coot: Model-building tools for molecular graphics. *Acta Crystallogr D Biol Crystallogr* 60(Pt 12 Pt 1):2126–2132.
53. Lebedev AA, et al. (2012) JLigand: A graphical tool for the CCP4 template-restraint library. *Acta Crystallogr D Biol Crystallogr* 68(Pt 4):431–440.
54. Laskowski RA, Swindells MB (2011) LigPlot+: Multiple ligand-protein interaction diagrams for drug discovery. *J Chem Inf Model* 51(10):2778–2786.
55. Sievers F, et al. (2011) Fast, scalable generation of high-quality protein multiple sequence alignments using Clustal Omega. *Mol Syst Biol* 7:539.
56. Warman AJ, et al. (2013) Antitubercular pharmacodynamics of phenothiazines. *J Antimicrob Chemother* 68(4):869–880.
57. Nilsen A, et al. (2014) Discovery, synthesis, and optimization of antimalarial 4(1H)-quinolone-3-diarylethers. *J Med Chem* 57(9):3818–3834.
58. Liu ZD, et al. (2001) Synthesis of 2-amido-3-hydroxypyridin-4(1H)-ones: Novel iron chelators with enhanced pFe3+ values. *Bioorg Med Chem* 9(3):563–573.
59. Halgren TA (1996) Merck molecular force field. I. Basis, form, scope, parameterization, and performance of MMFF94. *J Comput Chem* 17:490–519.
60. Jones G, Willett P, Glen RC, Leach AR, Taylor R (1997) Development and validation of a genetic algorithm for flexible docking. *J Mol Biol* 267(3):727–748.
61. Verdonk ML, Cole JC, Hartshorn MJ, Murray CW, Taylor RD (2003) Improved protein-ligand docking using GOLD. *Proteins* 52(4):609–623.
62. Jones G, Willett P, Glen RC (1995) Molecular recognition of receptor sites using a genetic algorithm with a description of desolvation. *J Mol Biol* 245(1):43–53.